Supporting Information

Nicolet et al. 10.1073/pnas.0904385106

SI Text

1. Enzyme Models. When the X-ray structures of the unreacted and the cleaved form of AdoMet are superimposed, the main differences reside at the active site. We built all models from the X-ray structure of the cleaved form which was solved at a higher resolution. The active site of the unreacted form was superimposed onto its counterpart in the cleaved form. Structural waters were included in our model as they are well conserved in both crystal structures.

The Schrödinger Suite [Schrödinger, LLC, New York, 2008] was used for all modeling and simulations of the enzyme models. Missing heavy and hydrogen atoms were constructed using the Maestro program. The positions of hydrogen atoms were optimized keeping the heavy atom positions fixed. Hybrid quantum mechanical (QM)/molecular mechanical (MM) potentials were used to model the whole enzyme. The following 120 atoms of the active site were treated quantum mechanically 1) AdoMet or 5′-dA + Met, 2) the $[Fe_4S_4]$ cluster, 3) a water molecule connecting the carboxylate groups of AdoMet and Glu-161, 4) Glu-161 that anchors the ribose of AdoMet via a strong interaction with both hydroxyl groups, and 5) Cys-63, Cys-67, and Cys-70 which are ligands to the $[Fe_4S_4]$ cluster.

In $[Fe_4S_4]$ clusters, the iron ions exhibit local high spin configurations $S(Fe^{III}) = 5/2$ (ferric) and $S(Fe^{II}) = 2$ (ferrous). The oxidized + 2 cluster state consists of two mixed-valence iron pairs (Fe^{II}-Fe^{III}) of spin S = 9/2 each. These pairs' spins are antiferromagnetically coupled, yielding a total cluster spin S = 0. In the reduced + 1 state, there is one mixed-valence (Fe^{II}-Fe^{III}) pair, as well as a ferrous pair (Fe^{II}-Fe^{II}) of spin S = 4. These two pairs are again antiferromagnetically coupled, yielding a total cluster spin S = 1/2 [we know from an EPR study on HydE that the reduced cluster is low spin S = 1/2 (1)].

The high-spin (HS) state S = 17/2 (see Fig. S1*B*: all iron resulting spins are parallel) of reduced $[Fe_4S_4]$ clusters can be easily approximated computationally. By contrast, the low spin S = 1/2 cluster state cannot be computed with conventional mono-determinantal DFT methods. To circumvent this problem, a standard procedure consists in computing instead broken symmetry (BS) states which are not pure spin states but states of mixed-spin (Ms = 1/2) and spatial broken symmetries allowing for spin localization onto the iron sites (see Fig. S1*B*). Finally, due to the coordination of the cluster (3 Cys + AdoMet or Met) the iron sites are not equivalent. We therefore tested several pair combinations where the unique iron involved (Fe4*) belongs either to the mixed valence or to the ferrous pair. Among the six possible configurations, the energetically most stable one corresponds to the unique iron ion being ferrous (see Fig. S1*C*).

Link atoms were used to model the interface between the QM and the MM parts of Cys-63, Cys-67, Cys-70, and Glu-161. Four models were constructed (AdoMet + $[Fe_4S_4]^{2+}$) and (5′-dA + Met + $[Fe_4S_4]^{2+}$) that correspond to the X-ray structures and (AdoMet + $[Fe_4S_4]^{1+}$) and (5′-dA + $[Fe_4S_4]^{2+}$) to model the reactant and the product of the AdoMet cleavage, respectively.

2. Transition State Search. The geometries of the four models were optimized on the QM/MM potential surface; first, the QM part was kept fixed and the MM part was optimized with a decreasing harmonic constraint from 6.0 to 1.2 $kJ.Å^{-2}.mol^{-1}$); second, the QM/MM system was optimized holding the MM atoms located beyond 13 Å of the QM part fixed. The optimized structures of the reactant and the product were used to determine the transition state leading to the electron transfer from the cluster to AdoMet using the linear synchronous transit method implemented in the Schrödinger Suite. Single-point energies were calculated for the reactant (R), the product (P), and the transition state (TS) structures.

3. Small Model Systems. An electron transfer process requires both energy matching (the so-called nuclear factor) and non-zero overlap (the so-called electronic factor) between the occupied donor (D) and empty acceptor (A) localized electronic orbitals. Within a simple valence-bond framework, the interaction between D and A results into an occupied orbital : D - (σ/2)A and an empty one: A - (σ/2)D, where $\sigma = <D\ A>$ (overlap). We thus looked for two molecular orbitals, one occupied (HOMO, or close to it) and one empty (LUMO, or close to it), resulting from the interaction of the putative donor and acceptor orbitals.

We computed the BS states for the R, P, and TS structures (2). As an example, the HOMO of the R state is mainly composed of Fe4* d orbitals with a minor contribution from the other ferrous iron Fe2 (Fig. S1). It bears the reducing electron belonging to the minority α spin (see Fig. S1*B*). Its spin density distribution will serve as an index providing insight into the extent of its delocalization and therefore into the identity of the acceptor orbital. However, due to the hybrid (QM/MM) modeling of the systems, the perturbation generated at the interface precludes any characterization of the LUMO*s*.

To circumvent that problem and still get some information from the LUMOs of the reactant, we constructed a small 'pure' QM model by extracting the active site from the QM/MM optimized structure of R (model a: see Fig. S2*A*). The HOMO/LUMO orbitals of this reactant model will give an indication as to where (from and to) the reducing electron will preferentially be transferred. For the sake of comparison, we also constructed a second model (see Fig. S2*B*) based on the crystal structure of SAH-bound HydE (4) where the SAH is in the same position as the AdoMet (see *Main Text*) at the active site (model b). The main difference between the two minimal models is the charge of the sulfur atom that goes from + 1 (a) to 0 (b).

SI Results

1. X-Ray Structures of AdoMet-Bound Radical AdoMet Proteins. We were unable to obtain higher than 50% occupancy of AdoMet in our crystals. The remaining 50% occupancy corresponds to SAH which is a major product of the hydrolysis of AdoMet at pH 8.0 (that most likely occurred during the crystallization experiment). However, there is no significant difference between the AdoMet- and SAH-binding modes in the HydE structure (3). Therefore, we modeled an AdoMet molecule bound to the cluster and we applied 50% and 100% occupancies to the methyl group and the rest of the AdoMet atoms, respectively. This model gives a similar temperature factor distribution for the AdoMet atoms in our 1.62 Å structure and those of the SAH atoms in the original 1.35-Å resolution structure relative to all protein atoms (see Table S1). This confirms that there are no significant differences between the atom positions in AdoMet and SAH, except for the presence of an extra methyl group in the former and the orientation of the side chain of L305 (3). We found that the distance between the methyl carbon atom of AdoMet and the closest iron atoms of the $[Fe_4S_4]$ cluster is 4.0 Å (Fe4* and Fe1). In addition, the distances for the calculated methyl protons to the closest iron atoms are 3.0 (Fe1) and 3.5 Å (Fe4*). These values are in agreement with the ones found in an

ENDOR study of pyruvate formate-lyase activating enzyme (PFL-AE) (≈4–5 Å and ≈3.0 to 3.8 Å, respectively) (4).

We have compared the AdoMet binding modes in the available X-ray structures of coproporphyrinogen III oxidase (HemN) (5), biotin synthase (BioB) (6), lysine-2,3-aminomutase (LAM) (7), MoaA (8), PFL-AE (9), and HydE (this work). We used the conserved [Fe_4S_4] cluster of the five proteins as a reference for the superimposition. This clearly shows that AdoMet adopts the same binding mode to the cluster in all cases. A closer analysis indicates that HydE, MoaA, and LAM present exactly the same structure of the methionine moiety. On the other hand, BioB and HemN show slight deviations in the position of Cβ and Cγ. However, these changes do not affect the interactions with the cluster, as reported in Table 2. In addition, it seems that in the HemN X-ray structure, the [Fe_4S_4] cluster was refined with Fe-S distances shorter than the standard 2.3-Å value. To check this possibility we re-refined the HemN structure (PDB code 1OLT) with REFMAC after having placed the [Fe_4S_4] cluster atoms in the 2*Fo-Fc* electron density map provided by the electron density server (10) (EDS), using the real space refinement option of Coot (11). In the re-refined structure all of the Fe-S distances were about 2.3 Å and both the R_{cryst} and R_{free} improved from 0.154 to 0.147 and 0.187 to 0.184, respectively. The distances between AdoMet and the cluster then converged to values close to the ones observed for HydE, indicating similar interactions in the two proteins. According to a very recent study the same is true for PFL-AE (9).

2. Comparison of the AdoMet- and the [5′-dA + Met]-Bound X-Ray Structures of HydE. The root mean square deviation for the Cα atoms between the AdoMet-bound and the [5′-dA + Met]-bound structures is 0.14 Å. The most dramatic differences involve the methionine moiety that binds the [Fe_4S_4] cluster differently depending on whether the methionine is attached to the 5′-deoxyadenosyl part (AdoMet-bound, Fig. 2*A*) or is free ([5′-dA + Met]-bound, Fig. 2*B*). The water molecule network at the active site is the same in the two structures. In addition, we observe a slight rotation of the 5′-deoxyadenosyl moiety centered on the N6 atom of the base, moving the ribosyl moiety away from the methionine, resulting in a 1.41 Å shift of the C5′ atom. As already reported (3), the [Fe_4S_4] cluster in HydE with AdoMet bound is slightly distorted from ideal geometry. In the [5′-dA + Met] structure the unique Fe4* moves away from the rest of the cluster changing from an approximately tetrahedral to a nearly octahedral coordination. S3*-Fe4*, S1-Fe4*, and S4-Fe4* distances are 2.33, 2.35, and 2.28 Å and 2.44, 2.39, and 2.35 Å in the AdoMet and the [5′-dA + Met] forms, respectively.

3. X-Ray Structure of AdoMet Cleavage Products in MoaA. In 2006, the 2.35-Å resolution structure of MoaA in complex with its substrate 5′-GTP was solved after reduction of its iron sulfur clusters (12). The authors concluded that their structure corresponded to that of the active site after AdoMet cleavage. However, inspection of the electron density corresponding to the MoaA structure (PDB code 2FB3), does not favor the presence of the cleavage products. The reasons are the following:

1) In chain A of molecule 1, there is continuous electron density between the putative 5′-dA and Met moieties (ESD map), suggesting intact AdoMet binding; 2) surprisingly, the C5′ atom was found to be disordered. This is difficult to understand as C5′ is bound to the rather well-defined ribose ring and should move in concert with it. 3) In the authors' model, the C4′-Sδ distance is 2.67 Å, comparable to those in AdoMet-LAM, 2.87 Å; HydE, 2.91 Å; MoaA, 2.88 Å; BioB, 2.77 Å; and HemN, 3.24 Å where AdoMet was not cleaved. At a C4′-Sδ distance of 2.67 Å, there is no room to insert a non Sδ-bonded C5′. On the other hand, in our [5′-dA + Met] structure, the corresponding distance is 4.49 Å and likely represents the signature of AdoMet cleavage.

In the second MoaA molecule of the asymmetric unit, chain B, there is no electron density for either 5′-dA, Met or AdoMet, suggesting that under the experimental conditions either AdoMet or its products of cleavage may have left the active site as was proposed in BioB and PFL-AE (13).

4. Charge and Spin Analyses on QM/MM Models R, TS, and P (Table S2)

5. Analysis of the Small Models. For model a (Fig. S2*A*), with the B3LYP potential, the HOMO is similar to that of the whole QM/MM system: mainly composed of Fe4* with a small contribution from Fe2 but not from Sδ^+ which is surprising given the HOMO of the TS (Fig. 4*B*). The LUMO is mainly composed of Sδ^+ (pz) with small contributions from Fe2 and Fe4* (in that order). We report in Table S3 the Mulliken charge and spin population analysis for both QM models a and b. We expected a non-zero fraction of spin population delocalized onto the AdoMet sulfur atom. It is however very small (≈0.01, within error bars).

Using instead the VBP potential yields more delocalized orbitals; the 17% spin population present on the Sδ^+ atom is very significant. This is further confirmed by the character of the HOMO: Fe4* (≈56%), Fe2 (≈16%), and Sδ^+ (≈7%, pz), and the LUMO: Fe4* (14%), Fe2 (52%), and Sδ (8%, pz). With the B3LYP potential, the Sδ^+ pz character was localized within the LUMO whereas, with the VBP potential, the Sδ^+ pz character is spread over the first few lower empty molecular orbitals. The difference in character description between B3LYP and VBP is clearly seen when comparing charge and spin populations (Table S3 and Table S4). First, the charges are very different which is expected because atomic charges are not uniquely defined quantities and the choice of potential has therefore a drastic effect on the way charges are shared among atomic domains. By contrast, both sets of spin populations are consistent although the B3LYP population magnitudes are larger than VBP ones, illustrating the fact that B3LYP orbitals are more localized.

Our calculations point to the fact that Fe4* is the electron donor site and Sδ^+ the intermediary acceptor site. To rationalize this result, let us state that in 'regular' thiolate-coordinated iron-sulfur clusters, sulfur orbitals are energetically sandwiched between lower (majority spin) and higher (minority spin) iron orbitals (Fig. S3*A*), as it is commonly the case for standard iron-sulfur clusters (14). Superposed to these levels are the $(S\text{-}C)_{AdoMet}$ bonding-antibonding molecular orbitals (≈7 eV splitting). We verified computationally (Fig. S3*B*) that the antibonding orbital lies within the iron minority set bearing the reducing electron. By contrast, upon replacing the positively charged sulfonium by a neutral sulfur S_{SAH} (model b), the bonding-antibonding pair rises up in energy (Fig. S3*B*) and there is no longer any orbital interaction between the [Fe_4S_4] core, on the one hand, and S_{SAH} in the fourth ligand, on the other hand. The behavior of this model matches that of cysteines in standard iron-sulfur clusters. As a further check, the results obtained with ADF/VBP for model b show no spin population on the sulfur atom and no S_{AdoH} contribution to either HOMO or LUMO (Table S4).

1. Rubach JK, Brazzolotto X, Gaillard J, Fontecave M (2005) Biochemical characterization of the HydE and HydG iron-only hydrogenase maturation enzymes from Thermotoga maritima. *FEBS Lett* 579:5055–5060.

2. Morales R, Frey M, Mouesca JM (2002) An approach based on quantum chemistry calculations and structural analysis of a [2Fe-2S*] ferredoxin that reveal a redox-linked switch in the electron-transfer process to the Fd-NADP(+) reductase. *J Am Chem Soc* 124:6714–6722.

3. Nicolet Y, et al. (2008) X-ray structure of the [FeFe]-hydrogenase maturase hydE from *Thermotoga maritima*. *J Biol Chem* 283:18861–18872.
4. Walsby CJ, et al. (2002) Electron-nuclear double resonance spectroscopic evidence that *S*-adenosylmethionine binds in contact with the catalytically active [4Fe-4S](+) cluster of pyruvate formate-lyase activating enzyme. *J Am Chem Soc* 124:3143–3151.
5. Layer G, Moser J, Heinz DW, Jahn D, Schubert WD (2003) Crystal structure of coproporphyrinogen III oxidase reveals cofactor geometry of Radical SAM enzymes. *EMBO J* 22:6214–6224.
6. Berkovitch F, Nicolet Y, Wan JT, Jarrett JT, Drennan CL (2004) Crystal structure of biotin synthase, an *S*-adenosylmethionine-dependent radical enzyme. *Science* 303:76–79.
7. Lepore BW, Ruzicka FJ, Frey PA, Ringe D (2005) The X-ray crystal structure of lysine-2,3-aminomutase from *Clostridium subterminale*. *Proc Natl Acad Sci USA* 102:13819–13824.
8. Hanzelmann P, Schindelin H (2004) Crystal structure of the *S*-adenosylmethionine-dependent enzyme MoaA and its implications for molybdenum cofactor deficiency in humans. *Proc Natl Acad Sci USA* 101:12870–12875.
9. Vey JL, et al. (2008) Structural basis for glycyl radical formation by pyruvate formate-lyase activating enzyme. *Proc Natl Acad Sci USA* 105:16137–16141.
10. Kleywegt GJ, et al. (2004) The Uppsala electron-density server *Acta Crystallogr* 60:2240–2249.
11. Emsley P, Cowtan K (2004) Coot: Model-building tools for molecular graphics *Acta Crystallogr* 60:2126–2132.
12. Hanzelmann P, Schindelin H (2006) Binding of 5 ′-GTP to the C-terminal FeS cluster of the radical *S*-adenosylmethionine enzyme MoaA provides insights into its mechanism. *Proc Natl Acad Sci USA* 103:6829–6834.
13. Cosper MM, et al. (2003) Structural studies of the interaction of *S*-adenosylmethionine with the [4Fe-4S] clusters in biotin synthase and pyruvate formate-lyase activating enzyme. *Protein Sci* 12:1573–1577.
14. Noodleman L, Case DA (1992) Density-functional theory of spin polarization and spin coupling in iron-sulfur clusters. *Adv Inorg Chem* 38:423–470.
15. te Velde GT, Baerends EJ (1992) Numerical-integration for polyatomic systems. *J Comp Phys* 99:84–98.

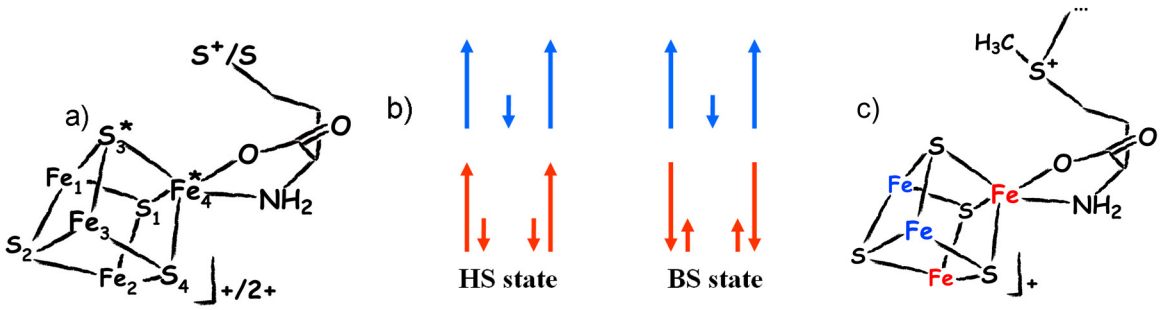

Fig. S1. (*A*) Names assigned for all atoms of the iron sulfur cluster (numbering as in PDB code 3CIW), Fe4* being the unique iron site, and S3* the sulfide ion postulated to be in interaction with the sulfonium from AdoMet (4). (*B*) Schematic representation of the spin systems in reduced [Fe_4S_4] clusters for both the high-spin (HS) state and the broken symmetry (BS) state (Ms = 1/2). Top (blue): the mixed-valence pair (Fe1-Fe3) of spin 9/2; bottom (red): the ferrous pair (Fe4*-Fe2) of spin 4. The large arrows represent so-called 'majority' spins (5/2) on each iron site whereas small arrows stand for 'minority' spins (1/2 each). (*C*) Iron valence combination within the reduced cluster that corresponds to the lowest energy state. The ferrous pair is shown in red while the mixed valence pair is depicted in blue (same color code as in Fig. S1*B*).

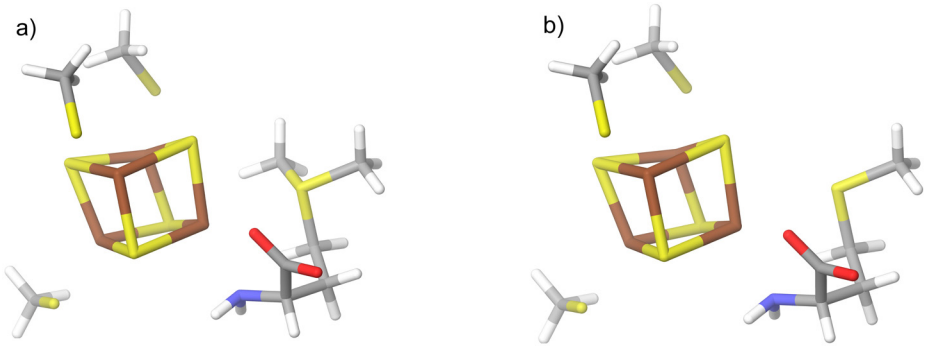

Fig. S2. Minimal models of the reduced $[Fe_4S_4]^{+1}$ coordinated by 3 cysteines and (*A*) *S*-methylmethionine (model a) or (*B*) methionine (model b).

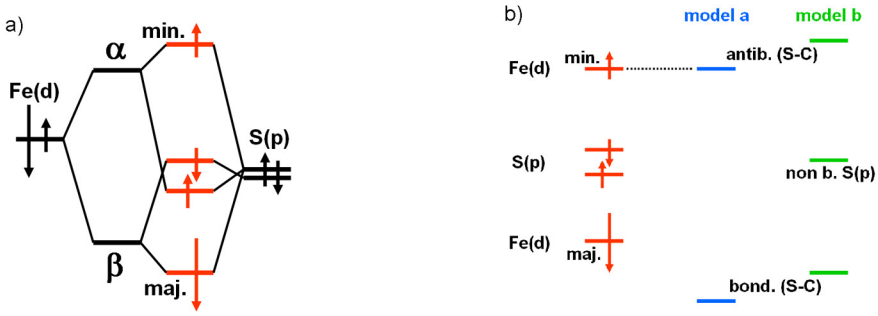

Fig. S3. (*A*) Typical schematic energy level diagram for a 'regular' iron-sulfur cluster showing the (thiolate ligand and inorganic core) sulfur orbitals sandwiched between those of the (mainly iron) minority spin (higher) and majority spin (lower) iron orbitals. α and β are spin up and down, respectively. (*B*) In blue are schematically represented the bonding-antibonding $(S\text{-}C)_{AdoMet}$ molecular orbitals from model a (sulfonium); same in green for the bonding-antibonding $(S\text{-}C)_{SAH}$ of model b (thioether). Labels: 'bond.' = bonding, 'antib.' = antibonding, and 'non b.' = non bonding (i.e., lone pair).

Table S1. Temperature-factor (square ångstroms) analysis of the AdoMet (this work) and SAH structures (ref. 3)

Coordinates	Average	St. Dev	Min	Max
AdoMet-HydE	17.29	9.40	6.77	69.15
AdoMet in AdoMet-HydE	14.09	1.47	12.44	17.19
SAH-HydE	19.35	8.97	8.56	73.43
SAH in SAH-HydE	14.52	1.62	12.56	19.09

Table S2. Charge (first line) and spin (second line) are given for each atom of the cluster and atoms C5′ and Sδ of AdoMet or Met

	Fe4*	S3*	S1	S2	S4	Fe1	Fe2	Fe3	C5′	Sδ
R	−0.06	−0.27	−0.28	−0.27	−0.33	−0.35	0.07	−0.06	−0.40	0.60
	−3.64	0.26	0.20	0.30	0.00	3.67	−3.51	3.58	0.00	0.01
TS	0.04	−0.18	−0.12	−0.18	−0.24	−0.30	−0.16	−0.03	−0.24	0.30
	−3.66	0.36	−0.03	0.02	−0.27	3.62	−3.58	3.57	1.04	−0.03
P	0.04	−0.18	−0.13	−0.19	−0.25	−0.26	−0.15	−0.03	−0.23	0.29
	−3.67	0.35	−0.01	0.01	−0.27	3.62	−3.59	3.58	1.05	−0.04

Table S3. Charge (first line) and spin (second line) analysis for the ″pure″ QM models a and b computed with the Jaguar code (Schrödinger Suite) (hybrid HF/DFT exchange-correlation potential B3LYP)

	Fe4*	S3*	S1	S2	S4	Fe1	Fe2	Fe3	C5′	Sδ
Model a (B3LYP)	−0.08	−0.24	−0.37	−0.22	−0.25	−0.03	0.00	−0.37	−0.47	0.67
	−3.61	0.24	0.17	0.33	−0.03	3.57	−3.50	3.65	0.00	0.01
Model b (B3LYP)	0.02	−0.23	−0.32	−0.30	−0.29	−0.06	−0.04	−0.31	−0.47	0.26
	−3.64	0.30	0.19	0.27	0.00	3.58	−3.50	3.65	−0.01	0.01

Table S4. Charge (first line) and spin (second line) analysis for the ″pure″ QM models a and b computed with the ADF code (16) (standard VBP DFT exchange-correlation potential)

	Fe4*	S3*	S1	S2	S4	Fe1	Fe2	Fe3	C5′	Sδ
Model a (VBP)	0.37	−0.37	−0.46	−0.34	−0.36	0.21	0.16	0.13	0.46	0.52
	−3.25	0.16	0.06	0.14	−0.02	3.44	−3.25	3.33	−0.01	0.17
Model b (VBP)	0.42	−0.38	−0.48	−0.43	−0.43	0.24	0.20	0.17	0.36	0.17
	−3.33	0.18	0.08	0.19	0.01	3.43	−3.08	3.36	−0.01	0.00